Dalton Transactions

PAPER

Cite this: *Dalton Trans.*, 2014, **43**, 16450

Discrete and polymeric Cu(II) complexes featuring substituted indazole ligands: their synthesis and structural chemistry†

Chris S. Hawes*‡ and Paul E. Kruger*

Received 9th August 2014,
Accepted 16th September 2014

DOI: 10.1039/c4dt02428a

www.rsc.org/dalton

Reported here are the syntheses of four indazole-based ligands and the structural characterisation of four Cu(II) complexes derived from them. The ligands 1-(2-pyridyl)-1*H*-indazole, **L1**, and 2-(2-pyridyl)-2*H*-indazole, **L2**, have been characterised by single crystal X-ray diffraction methods for the first time. The intramolecular structural changes within **L1** and **L2** that result from the transition from the 1*H* to the 2*H* electronic configuration have been delineated. The synthesis of 1*H*-indazole-6-carboxylic acid, **H_2L3**, and 1*H*-indazole-7-carboxylic acid, **H_2L4**, is fully described and the structure of **H_2L4·H_2O** determined. The structures of two discrete mononuclear complexes {[Cu(**L1**)$_2$(NO_3)]·NO_3·1.5H_2O}, **1**, and {[Cu(**L2**)$_2$(NO_3)]·NO_3}, **2**, have been determined and their molecular compositions corroborated by solution-based methods. Reaction of Cu(II) with **H_2L3** generates a 2D coordination polymer, [Cu_3(**HL3**)$_4$-(NO_3)$_2$(EtOH)$_2$]·3(C_6H_6)·2(H_2O), **3**, that features the archetypal [Cu_2(OAc)$_4$] paddlewheel motif and 1D channels; whereas reaction with **H_2L4** gives a discrete complex [Cu(**HL4**)$_2$]·H_2O·MeOH, **4**, in which hydrogen bonding interactions link indazole dimers *via* a water molecule to yield a 1D network.

Introduction

The utilisation of self-assembly processes to generate multi-molecular architectures from pre-designed building blocks through applying the principles of supramolecular chemistry has been an area of intense research over the last couple of decades.[1] Rational ligand design in supramolecular chemistry is of crucial importance, for as the study of complex coordination architectures matures, so does the need for more advanced ligand types, to help fulfil emerging roles for applications of metallo-supramolecular chemistry.[2]

Nitrogen heterocyclic ligands have been widely employed as ligands in the formation of metallo-supramolecular assemblies, owing to their well-understood coordination chemistry and ready availability.[3] Pyridine-based heterocyclic systems remain the 'bedrock' of nitrogen containing ligands used within supra-molecular and metallo-supramolecular chemistry,[4] while imidazole, pyrazine and pyrazole-based systems are becoming increasingly popular.[5] Less widely reported in the literature are examples incorporating more exotic heterocyclic systems, such as fused-ring derivatives and mixed-heteroatom cyclic species. Such ligands offer many unique design features not present in simple heterocyclic systems, such as unique ligand field parameters, donor atom variability and new synthetically-available substitution patterns.

Fusion of five- and six-membered rings provides access to a greater variety of divergent donor-atom geometries than are available from more traditional ligand cores, a pertinent consideration given the ongoing efforts to predict overall network structures based on ligand geometries and functionalities.[6] Metal complexes of azolate-type ligands such as pyrazole and imidazole are also well known to display excellent stability against hydrolysis, by virtue of the high pK_a of the N–H group.[7] This property makes them ideal candidates for the next generation of porous coordination polymer materials, for which hydrolytic stability is a crucial consideration. Nitrogen heterocycles such as indazole also have the inherent advantage, from a coordination chemistry point of view, of a well-established base of synthetic knowledge derived from the medicinal chemistry literature, allowing ready access to a wide range of substitution possibilities and established synthetic pathways to compounds of potential interest.[8] However, only relatively few examples of indazole-based coordination assemblies have been reported to date.[9,10]

MacDiarmid Institute for Advanced Materials and Nanotechnology, Department of Chemistry, University of Canterbury, Private Bag 4800, Christchurch 8140, New Zealand. E-mail: paul.kruger@canterbury.ac.nz

†Electronic supplementary information (ESI) available: Hydrogen bonding tables, thermogravimetric analysis plots, UV/Visible spectra for **L1** and **L2** and complexes **1** and **2**. CCDC 1018276–1018282. For ESI and crystallographic data in CIF or other electronic format see DOI: 10.1039/c4dt02428a

‡Current address: School of Chemistry, Monash University, Clayton, Victoria 3800, Australia. E-mail: chris.hawes@monash.edu

We have recently reported the syntheses of the first two examples of indazole-based coordination polymers, in which indazole-5-carboxylate and indazole-3-carboxylate both formed 3-dimensional networks on reaction with Cu(II) ions.[11,12] To further explore the utility of the indazole framework in metallo-supramolecular chemistry, we report here the synthesis of four substituted indazole derivatives containing pyridine or carboxylic acid functionality, and structural descriptions of their behaviour on coordination with Cu(II) ions in solution and in the solid state.

Experimental

General considerations

All solvents, reagents and starting materials were of reagent grade or better and were purchased from standard suppliers. NMR spectra were recorded on a Varian INOVA instrument operating at 500 MHz for ^{1}H and 126 MHz for ^{13}C using standard Varian pulse sequences. Mass spectra were recorded in positive ion electrospray ionisation mode with a Bruker MaXiS 3G UHR-TOF instrument with samples dissolved in HPLC-grade methanol or acetonitrile. UV/Visible spectra were recorded on a Varian CARY spectrometer using quartz cuvettes with 1 cm path length, with samples dissolved in acetonitrile or nitromethane as specified. Infrared spectra were recorded on a Perkin Elmer Spectrum One FTIR instrument operating in diffuse reflectance sampling mode with samples diluted in powdered KBr. Melting points were recorded on an Electrothermal melting point apparatus and are uncorrected. Thermogravimetric analysis was performed on a TA Instruments Q600 SDT DSC/TGA instrument where samples were heated on alumina crucibles under nitrogen flow of 100 mL min^{-1} and were heated at a rate of 1 °C min^{-1} to 500 °C. Elemental analyses were carried out by Campbell Microanalytical Laboratory, Department of Chemistry, Otago University, Dunedin, New Zealand.

X-ray crystallography

Refinement data are presented in Table 1. X-ray crystallographic data collection and refinement was carried out with an Oxford-Agilent SuperNova instrument with focused microsource Cu/Kα (λ = 1.5418 Å) radiation and ATLAS CCD area detector. All structures were solved using direct methods with SHELXS[13] refined on F^2 using all data by full matrix least-squares procedures with SHELXL-97[14] within OLEX-2.[15] Non-hydrogen atoms were refined with anisotropic displacement parameters. Hydrogen atoms were included in calculated positions with isotropic displacement parameters either 1.2 times or 1.5 times the isotropic equivalent of their carrier atoms, where appropriate, with the exception of selected hydrogen bonding sites, in which the hydrogen atoms were manually located from residual Fourier peaks and modelled with appropriate bond length restraints and U_{iso} dependences. The functions minimized were $\sum w(F_o^2 - F_c^2)$, with $w = [\sigma^2(F_o^2) + aP_2 + bP]^{-1}$, where $P = [\max(F_o)^2 + 2F_c^2]/3$. CCDC 1018276–1018282.

Table 1 Crystallographic data for compounds **L1**, **L2**, **L4** and complexes **1–4**

Compound reference	L1	L2	L4	1	2	3	4
Chemical formula	$C_{12}H_9N_3$	$C_{12}H_9N_3$	$2(C_8H_6N_2O_2)\cdot H_2O$	$2(C_{24}H_{18}CuN_7O_3)\cdot 2(NO_3)\cdot 3(H_2O)$	$C_{24}H_{18}CuN_7O_3\cdot NO_3$	$C_{36}H_{32}Cu_3N_{10}O_{16}\cdot 2.25(C_6H_6)\cdot 2(H_2O)$	$C_{16}H_{10}CuN_4O_4\cdot 0.5(C_2H_2O_2)\cdot H_2O$
Formula mass	195.22	195.22	342.31	1210.06	578.00	1263.11	435.88
Crystal system	Orthorhombic	Orthorhombic	Triclinic	Monoclinic	Monoclinic	Triclinic	Monoclinic
a/Å	5.0020(6)	5.6717(6)	4.9524(7)	7.2872(2)	18.0728(19)	10.2213(6)	25.730(2)
b/Å	13.078(2)	11.2569(11)	10.9756(9)	15.9102(5)	7.5078(6)	11.4215(5)	4.5836(2)
c/Å	14.257(2)	14.8452(16)	14.6313(15)	21.2623(6)	18.9452(19)	14.0872(7)	17.8406(13)
α/°	90.00	90.00	81.698(8)	90.00	90.00	105.934(4)	90.00
β/°	90.00	90.00	83.854(10)	99.328(3)	115.277(13)	101.559(4)	124.140(11)
γ/°	90.00	90.00	78.805(9)	90.00	90.00	104.354(4)	90.00
Unit cell volume/Å^3	932.6(2)	947.80(17)	769.43(15)	2432.58(13)	2324.5(4)	1467.04(13)	1741.5(2)
Temperature/K	120.0(1)	120.0(1)	120.0(1)	120.0(1)	120.0(1)	120.0(1)	120.0(1)
Space group	$P2_12_12_1$	$P2_12_12_1$	$P\bar{1}$	$P2_1/n$	$P2_1/c$	$P\bar{1}$	$C2/c$
No. of formula units per unit cell, Z	4	4	2	2	4	1	4
No. of reflections measured	3567	4592	4768	9042	9123	22 189	5385
No. of independent reflections	1742	1734	2964	4759	4575	5737	1742
R_{int}	0.0169	0.0257	0.0262	0.0287	0.0391	0.0336	0.0264
Final R_1 values ($I > 2\sigma(I)$)	0.0335	0.0401	0.0428	0.0554	0.0519	0.0549	0.0433
Final $wR(F^2)$ values ($I > 2\sigma(I)$)	0.0877	0.0944	0.1079	0.1387	0.1354	0.1550	0.1197
Final R_1 values (all data)	0.0360	0.0494	0.0524	0.0744	0.0656	0.0624	0.0455
Final $wR(F^2)$ values (all data)	0.0894	0.1025	0.1158	0.1536	0.1458	0.1646	0.1215

Synthesis of 1-(2-pyridyl)-1*H*-indazole (L1) and 2-(2-pyridyl)-2*H*-indazole (L2)

Indazole (1.0 g; 8.5 mmol) was dissolved in 10 mL of anhydrous DMF under a nitrogen atmosphere at 0 °C. NaH was added in portions to this solution (490 mg; 10 mmol, 50% dispersion in oil) and the resulting mixture stirred for 30 minutes at 0 °C. 2-Bromopyridine (900 μL; 9.4 mmol) was then added and the mixture heated with stirring at 110 °C for 48 h. The cooled mixture was then poured into 100 mL water and extracted with CH_2Cl_2 (4 × 20 mL). The organic layers were concentrated *in vacuo* to give a brown residue which was taken up in 10 mL 50% aqueous HCl, washed with several portions of petroleum ether, filtered and neutralised with K_2CO_3. The resulting suspension was extracted with CH_2Cl_2 (4 × 10 mL) and the organic phase dried and evaporated to yield an orange oily residue of both **L1** and **L2**. The oil was subjected to flash chromatography using ethyl acetate–petroleum ether (1 : 1) on silica gel and the fraction containing **L1** and **L2** evaporated to dryness and further chromatographed using toluene–petroleum ether (1 : 1) on alumina to yield **L1** and **L2** separately. Combined yield 450 mg, 27%.

Analytical data for L1. Yield 230 mg, 14%; mp 71–74 °C; δ_H (500 MHz, $CDCl_3$): 7.16 (dd, 1H, J = 7.2, 4.8 Hz, H^4), 7.29 (t, 1H, J = 7.7 Hz H^7), 7.53 (dd, 1H, J = 8.4, 7.5 Hz, H^8), 7.78 (d, 2H, J = 7.9 Hz, H^6), 7.84 (ddd, 1H, J = 8.3, 7.2, 1.2 Hz, H^3), 8.06 (d, 1H, J = 8.4 Hz, H^2), 8.21 (s, 1H, H^1), 8.54 (dd, 1H, J = 4.6, 1.2 Hz, H^5), 8.86 (d, 1H, J = 8.6 Hz, H^9); δ_c (125 MHz, $CDCl_3$): 113.7, 115.5, 120.1, 120.9, 122.7, 126.2, 128.1, 137.0, 138.5, 139.1, 147.9, 154.5; HRMS-ESI m/z: found: 196.0872; $C_{12}H_{10}N_3$ requires: 196.0869 [M + H^+]; $\bar{\nu}_{max}$/cm^{-1} (KBr): 3550 m, 3410 m, 1616 s, 1587 s, 1500 s, 1479 s, 1451 s, 1353 m, 1199 s, 1145 m, 1078 m, 1010 s, 978 s, 778 s, 627 s.

Analytical data for L2. Yield 220 mg, 13%; mp 87–93 °C; δ_H (500 MHz, $CDCl_3$): 7.09 (t, 1H, J = 7.0 Hz, H^3), 7.28–7.33 (m, 2H, H^5 & H^8), 7.71–7.75 (m, 2H, H^2 & H^4), 7.89 (dt, 1H, J = 7.9, 1.8 Hz, H^7), 8.28 (d, 1H, J = 8.0 Hz, H^6), 8.50 (d, 1H, J = 3.9 Hz, H^9), 9.10 (s, 1H, H^1); δ_c (125 MHz, $CDCl_3$): 114.3, 118.3, 120.8, 121.5, 122.6, 122.9, 123.0, 127.8, 139.1, 148.6, 150.5, 152.1; HRMS-ESI m/z: found: 196.0877; $C_{12}H_{10}N_3$ requires: 196.0869 [M + H^+]; $\bar{\nu}_{max}$/cm^{-1} (KBr): 3058 m, 1911 m, 1790 m, 1592 s, 1517 s, 1474 s, 1434 s, 1374 m, 1350 m, 1313 m, 1199 s, 1146 s, 1056 s, 956 m, 907 m, 758 s.

Synthesis of methyl 1-acetyl-indazole-6-carboxylate, MeL3Ac

Methyl-3-amino-4-methylbenzoate (1.5 g; 9.1 mmol) was added to potassium acetate (460 mg; 4.7 mmol) in 50 mL anhydrous toluene and the mixture heated to reflux under a nitrogen atmosphere. Acetic anhydride (2.8 mL; 30 μmol) was added in one portion to the refluxing mixture, followed by the dropwise addition of isoamyl nitrite (1.86 mL; 14 mmol) over a period of 30 min. The mixture was then heated at reflux overnight, cooled to RT and filtered. The precipitate was washed several times with toluene, and the combined filtrates were evaporated to dryness to give a brown solid which was washed with several portions of petroleum ether and a small quantity of cold water and dried *in vacuo* to give a white microcrystalline solid. Yield 1.2 g, 61%. mp 162–164 °C; δ_H (500 MHz, $CDCl_3$): 2.81 (d, 1H, J = 1.3 Hz, H^1), 3.97 (d, 1H, J = 1.6 Hz, H^5), 7.78 (dd, 1H, J = 8.6, 0.8 Hz, H^4), 8.04 (dd, 1H, J = 8.4, 1.3 Hz, H^3), 8.17 (s, 1H, H^6), 9.11 (s, 1H, H^2); δ_C (125 MHz, $CDCl_3$): 23.3, 52.7, 117.5, 121.0, 125.6, 129.2, 131.3, 138.9, 139.5, 167.0, 171.2; HRMS-ESI m/z: found: 219.0761; $C_{11}H_{11}N_2O_3$ requires: 219.0764 [M + H^+]; $\bar{\nu}_{max}$/cm^{-1} (KBr): 2960 m, 1709 s br, 1587 m, 1416 m, 1294 m, 1246 s, 1201 m, 1139 m, 1093 w, 1034 w, 969 m, 942 s, 899 m, 741 m.

Synthesis of 1*H*-indazole-6-carboxylic acid, H_2L3

MeL3Ac (1.0 g; 4.6 mmol) was dissolved in 40 mL THF, and this solution was added to a 40 mL aqueous solution of lithium hydroxide (5.0 g; 210 mmol). The resulting suspension was heated at reflux with vigorous stirring overnight, after which time the solution was concentrated under vacuum to remove the organic phase. The resulting solution was filtered, adjusted to pH 3 with conc. HCl, to precipitate the product as a pale brown solid, which was filtered, washed with water and dried under vacuum. Yield 315 mg, 43%. mp 292–296 °C (decomp); δ_H (500 MHz, d_6-DMSO): 7.67 (dd, 1H, J = 8.3, 1.0 Hz, H^4), 7.85 (dd, 1H, J = 8.3, 0.8 Hz, H^3), 8.15 (s, 1H, H^6), 8.18 (d, 1H, J = 0.8 Hz, H^2), 13.24 (br s, 2H, H^1 & H^5); δ_C (125 MHz, CD_3OD): 114.1, 122.0, 122.6, 127.1, 130.6, 135.2, 141.4, 170.4; HRMS-ESI m/z: found: 163.0503; $C_8H_7N_2O_2$ requires: 163.0502 [M + H^+]; $\bar{\nu}_{max}$/cm^{-1} (KBr): 3258 br, 2864 br, 2582 br, 1679 s, 1579 m, 1518 m, 1425 m, 1230 s, 1087 m, 954 s, 857 m, 762 m, 693 m.

Synthesis of 1*H*-indazole-7-carboxylic acid, H_2L4

To 60 mL anhydrous toluene under a nitrogen atmosphere was added methyl-2-amino-3-methylbenzoate (1.8 g, 11 mmol) and KOAc (560 mg, 5.7 mmol), and the mixture heated to reflux, at which time acetic anhydride (3.2 mL, 34 mmol) was added and the mixture stirred at reflux for 10 min. Isoamyl nitrite (2.3 mL, 18 mmol) was added over 30 min and the mixture refluxed overnight. On cooling, the mixture was filtered and evaporated to dryness to give 1.6 g of a pale brown solid, which analysed for methyl 1*H*-indazole-7-carboxylate. This material was taken up in 40 mL THF, added to a solution of LiOH (5 g, 210 mmol) in 40 mL water, and heated at reflux for 48 h. On cooling, the mixture was concentrated on a rotary evaporator and the resulting aqueous phase filtered and adjusted to pH 4 with dilute HCl, to precipitate the product, which was filtered, washed with water and dried under vacuum. Yield 810 mg, 45%; mp 218–222 °C (decomp); δ_H (500 MHz, d_6-DMSO): 7.23 (t, 1H, J = 7.5 Hz, H^4), 7.97 (dd, 1H, J = 7.5, 1.0 Hz, H^3), 8.06 (dd, 1H, J = 7.8, 0.8 Hz, H^5), 8.21 (s, 1H, H^2), 13.1 (br s, 2H, H^1 & H^6); δ_c (125 MHz, d_6-DMSO): 113.7, 120.1, 124.6, 126.5, 129.0, 134.3, 138.0, 167.0; HRMS-ESI m/z: found: 163.0503; $C_8H_7N_2O_2$ requires: 163.0502 [M + H^+]; $\bar{\nu}_{max}$/cm^{-1} (KBr): 3316 s br, 1700 s, 1619 m, 1592 m, 1509 m, 1285 s, 1201 m, 1145 m, 1078 m, 1056 w, 943 m, 858 s, 745 s, 638 m, 601 m.

Synthesis of $[Cu(L1)_2NO_3]\cdot NO_3\cdot 1.5H_2O$, 1

L1 (10 mg; 51 μmol) and $CuNO_3\cdot 3H_2O$ (6.0 mg; 35 μmol) were combined in 5 mL $MeNO_2$ which was stirred with gentle heating for 5 min and filtered. The filtrate was subjected to diffusion of benzene vapour which deposited green crystals of **1** within one week. Yield 4.2 mg, 28%. mp 233–235 °C (decomp); found: C, 47.5; H, 3.27; N, 18.4%; $C_{24}H_{18}N_8O_6Cu\cdot 1.5H_2O$ requires: C, 47.6; H, 3.50; N, 18.5%; HRMS-ESI *m*/*z* (MeCN): found: 226.5438; $C_{24}H_{18}N_6Cu$ requires: 226.5439 [M^{2+}]; λ_{max}/nm, ($MeNO_2$): 720 (215 M^{-1} cm^{-1}); $\bar{\nu}_{max}$/cm^{-1} (KBr): 3514 m, 1617 m, 1476 s, 1437 m, 1349 s, 1298 s, 1214 m, 1155 m, 1091 w, 1055 w, 913 w, 773 s, 746 s, 615 m.

Synthesis of $[Cu(L2)_2NO_3]\cdot NO_3$, 2

L2 (10 mg; 51 μmol) and $CuNO_3\cdot 3H_2O$ (6.0 mg; 25 μmol) were combined in 5 mL $MeNO_2$, which was stirred with gentle heating for 5 min and filtered. The filtrate was subjected to diffusion of toluene vapour, which deposited green crystals of **2** over several days. Yield 6.0 mg; 42%; mp 254–255 °C (decomp); found: C, 49.9; H, 3.07; N, 19.4%; $C_{24}H_{18}N_8O_6Cu$ requires: C, 49.9; H, 3.14; N, 19.4%; HRMS-ESI *m*/*z* (MeCN): found: 226.5438, $C_{24}H_{18}N_6Cu$ requires: 226.5439 [M^{2+}]; λ_{max}/nm, ($MeNO_2$): 750 (230 M^{-1} cm^{-1}); $\bar{\nu}_{max}$/cm^{-1} (KBr): 3073 m, 1630 m, 1575 m, 1521 s, 1450 s, 1327 s, 1300 s, 1278 m, 1150 w, 1025 m, 814 m, 764 s.

Synthesis of $[Cu_3(HL3)_4(NO_3)_2(EtOH)_2]\cdot 3C_6H_6\cdot 2H_2O$, 3

To a solution of H_2L3 (10 mg; 62 μmol) in 5 mL EtOH was added $CuNO_3\cdot 3H_2O$ (11 mg; 44 μmol) and the mixture stirred with gentle heating for 10 min. The mixture was filtered and the filtrate subjected to diffusion of benzene vapour, which deposited blue/green crystals of **3** within one month. Yield 3.6 mg, 18%; mp >300 °C; found: C, 39.3; H, 2.95; N, 12.4%; $C_{36}H_{32}N_{10}O_{16}Cu_3\cdot 3H_2O$ requires: C, 39.1; H, 3.46; N, 12.7%; $\bar{\nu}_{max}$/cm^{-1} (KBr): 3285 m br, 2921 m br, 1679 w 1610 w, 1577 m, 1514 m, 1410 s, 1360 s, 1223 m, 1094 w, 968 s, 675 m.

Synthesis of $[Cu(HL4)_2]\cdot H_2O\cdot MeOH$, 4

H_2L4 (10 mg; 61 μmol) was dissolved in 10 mL MeOH, to which was added $CuNO_3\cdot 3H_2O$ (7.0 mg; 28 μmol). The resulting mixture was stirred with gentle heating for 10 min and filtered. Purple rod crystals formed in the filtrate within 3 days and were isolated by filtration. Yield 5.1 mg, 43%; mp >300 °C; found: C, 47.2; H, 3.26; N, 13.2%; $C_{17}H_{13}N_4O_6Cu$ requires: C, 47.2; H, 3.03; N, 12.9%; $\bar{\nu}_{max}$/cm^{-1} (KBr): 2929 m br, 1633 s, 1596 s, 1517 w, 1448 m, 1357 s, 1326 m, 1190 m, 1153 w, 1122 w, 1035 m, 989 m, 876 m, 852 s, 765 s, 515 m.

Results and discussion

Synthesis and structural characterisation of L1 and L2

Substitution at the 1- and 2-positions of the indazole ring was achieved by reacting indazole with 2-bromopyridine in anhydrous DMF following deprotonation with NaH. Not surprisingly, this led to the isolation of a mixture of the two isomers, 1-(2-pyridyl)-1*H*-indazole, **L1**, and 2-(2-pyridyl)-2*H*-indazole, **L2**.[10] **L1** and **L2** were separated by column chromatography to afford sufficient quantities of each to allow an investigation into their coordination chemistry to be undertaken. A previous study[16] into the use of **L1** as a ligand did not report any structural characterisation of the ligand or any derived complexes and no reports detail the structures of **L2** complexes.

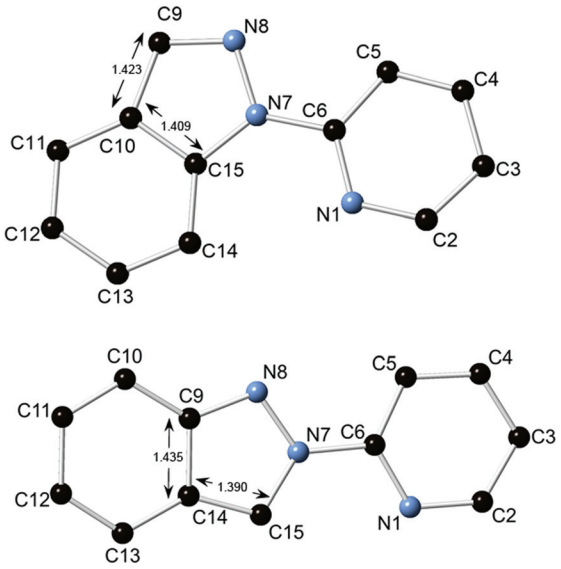

Fig. 1 Structure of ligands **L1** (top) and **L2** (bottom) with atom labelling scheme and selected bond length measurements (Å) highlighted. Hydrogen atoms omitted for clarity.

L1 and **L2** were crystallised by slow evaporation of the 50% toluene–petroleum ether eluent. Both crystal structures were solved and refined in the orthorhombic space group $P2_12_12_1$ and crystallographic data are detailed in Table 1. The structures of **L1** and **L2** both display the expected[17] *trans*-coplanar orientations of the pyridine–indazole system, Fig. 1. The most conspicuous intermolecular contacts are the offset face-to-face π–π interactions with mean interplanar distances 3.36 and 3.35 Å for **L1** and **L2**, respectively.

Of more interest is the degree of bond localisation present in each of the structures. Unsubstituted indazole compounds are known to favour the 1*H* electronic configuration[18] as this allows for greater electron delocalisation into the phenyl ring, compared to the 2*H* electronic configuration where the phenyl ring adopts an *ortho*-quinone-type electronic configuration. Partial bond localisation is expected to be most visible in **L1** (and separate from electronegativity considerations due to proximity of the pyridine ring) in the bond between the indazole 3-position, C9, and the adjacent ring junction carbon atom C10 (*cf.* C14–C15 bond in **L2**). The longer C9–C10 (1.423(3) Å) bond contains more single bond character in **L1**, whereas the shorter C14–C15 bond in **L2** reveals more double bond character (1.390(3) Å), the values falling well outside of 3σ of one another confirming a genuine variation. Likewise, the ring junction bond in **L2** is slightly longer (C9–C14 1.435(3) Å) than the corresponding bond in the more delocalised **L1**

(C10–C15 1.409(3) Å), with the effect reducing in magnitude with greater distance away from the five-membered ring.

Interestingly, the structure of **L1** can be compared to that of the related compound 3-(2-pyridyl)imidazo[1,5-*a*]pyridine, which crystallises in an isostructural fashion and contains equivalent intermolecular interactions.[19] In this case, replacement of a ring junction carbon atom with a nitrogen atom leads to a greater degree of bond localisation, akin to that observed in **L2** and leading to a comparable carbon–carbon bond distance in the imidazole ring of 1.391(6) Å.

Synthesis and characterisation of H_2L3 and H_2L4

The ligands 1*H*-indazole-6-carboxylic acid, H_2L3, and 1*H*-indazole-7-carboxylic acid, H_2L4, were prepared by a Jacobsen-type synthesis,[20] as we recently described for the synthesis of the 5-carboxylic acid isomer.[11] The relevant precursors were prepared by reduction of the appropriate isomers of methyl nitrotoluate, Scheme 1. For H_2L3 the product of the cyclisation is the *N*-acetyl ester, **MeL3Ac**, which was then deprotected under basic conditions. The methyl ester **MeHL4** was obtained by an equivalent reaction and used without purification, as the *N*-acetyl group was cleaved during the cyclisation, most likely facilitated by the steric interference of the adjacent methyl ester, which was subsequently cleaved to give H_2L4.

H_2L4 was crystallised by slow evaporation from a methanol solution, and the diffraction data solved and the structure refined in the monoclinic space group $P\bar{1}$ with crystallographic data detailed in Table 1. The asymmetric unit was found to contain two molecules of H_2L4 and one water molecule. Structurally, the two units of H_2L4 are nearly identical and exist in the 1*H*-configuration. As might be anticipated from a molecule replete with hydrogen bond donors and acceptors, hydrogen bonding interactions dominate the solid state structure of H_2L4, Fig. 2. The lattice water molecule participates in four such interactions, receiving two hydrogen bonds from the two non-equivalent carboxylic acid O–H groups, and donating two hydrogen bonds to the non-equivalent indazole nitrogen atoms. Each H_2L4 unit participates in reciprocal hydrogen bond interactions between the indazole N–H groups and carboxylate oxygen atoms of adjacent, crystallographically equivalent molecules. A zig-zag 1D polymer results from the combination of these hydrogen bond interactions.

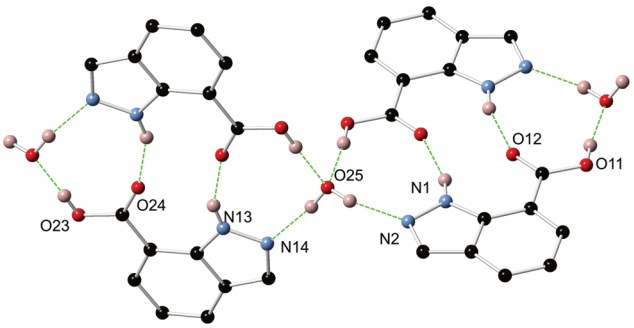

Fig. 2 Structure of H_2L4 with heteroatom labelling scheme, showing hydrogen bonding interactions between equivalent ligand molecules and lattice water molecule. Selected hydrogen atoms omitted for clarity.

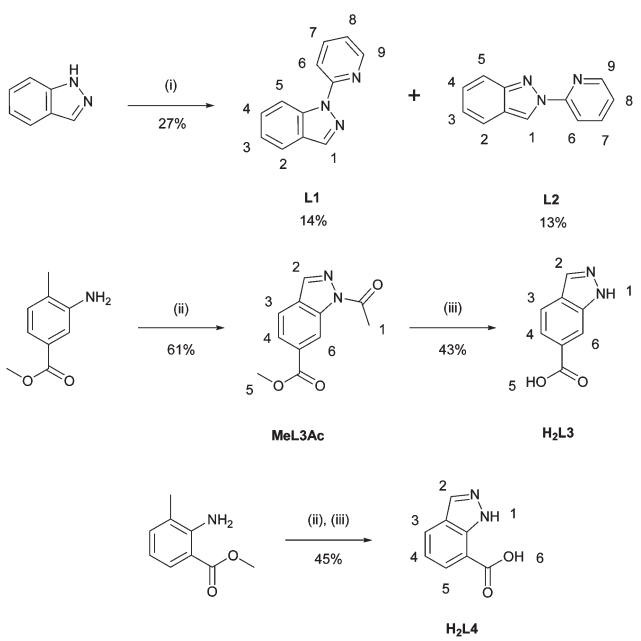

Scheme 1 Synthesis and structure of ligands **L1**–H_2L4 with ^{1}H NMR labelling schemes. Reagents and conditions: (i) NaH, 2-bromopyridine, DMF, 110 °C, 48 h; (ii) Ac_2O, isoamyl nitrite, KOAc, PhMe, reflux 18 h; (iii) LiOH, THF–H_2O, 48 h; $HCl_{(aq)}$.

Synthesis and characterisation of Cu(II) complexes of L1 and L2: $[Cu(L1)_2NO_3]\cdot NO_3\cdot 1.5H_2O$, 1, and $[Cu(L2)_2NO_3]\cdot NO_3$, 2

Ligands **L1** and **L2** were reacted separately with $Cu(NO_3)_2\cdot 3H_2O$ in nitromethane to give green solutions from which **1** and **2** crystallised following diffusion of benzene and toluene, respectively. These crystals are readily soluble in nitromethane solution and their UV/visible spectra found to display similarly broad d–d transitions ($\varepsilon \sim 200$ M^{-1} cm^{-1}) centred at 720 and 750 nm for **1** and **2**, respectively.[21] Likewise, electrospray ionisation mass spectrometry from acetonitrile solution identified a doubly charged peak at m/z 226.5438 for both **1** and **2**, ascribed to the presence of a $[Cu(L)_2]^{2+}$ species.

X-ray crystal structure of 1

The crystal structure of **1** was solved and refined in the monoclinic space group $P2_1/n$ and crystallographic data are detailed in Table 1. The asymmetric unit contains a five coordinate Cu(II) ion with trigonal bipyramidal geometry ($\tau = 0.66$)[22] where coordination is furnished by two bidentate **L1** ligands, with two pyridine and two indazole nitrogen atoms in the axial and equatorial positions, respectively. A weakly coordinating nitrate anion (Cu1–O 2.310(3) Å) completes the coordination sphere. Both ligands are approximately planar, with the pyridine–indazole interplanar angles 4.6 and 5.7°, Fig. 3.

The intermolecular contacts in **1** are dominated by π–π stacking interactions. Adjacent complexes align such that the non-coordinating oxygen atom of the coordinated nitrate anion points towards the metal ion of an adjacent complex,

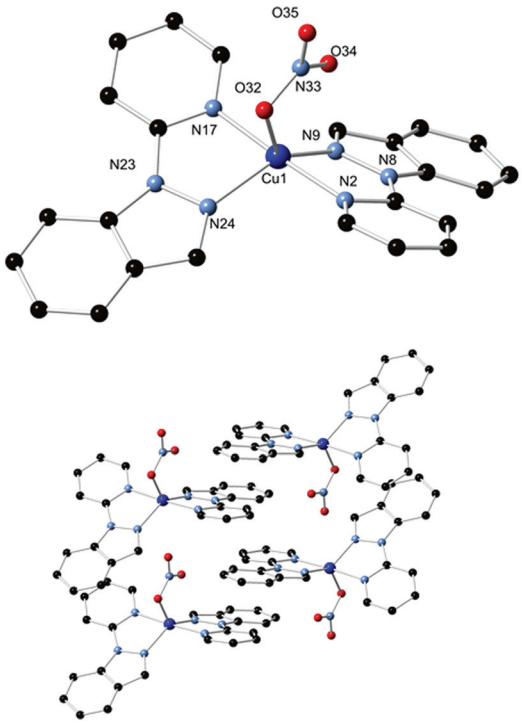

Fig. 3 Structure of **1** with heteroatom labelling scheme (top). Intermolecular interactions in **1** (bottom). Hydrogen atoms, lattice water molecules and non-coordinating nitrate anions omitted for clarity.

with a long O35···Cu1 distance of 3.246(3) Å, which results in the formation of a one-dimensional chain that runs parallel to the *a* unit cell axis. Adjacent chains align such that **L1** molecules interdigitate with mean interplanar distances of 3.35 and 3.42 Å for the two types of interaction, Fig. 3.

X-ray crystal structure of 2

The structure of **2** was determined in the monoclinic space group $P2_1/c$ and crystallographic data are detailed in Table 1. asymmetric unit contains a five coordinate Cu(II) ion with square-pyramidal geometry (τ = 0.16)[22] where coordination is furnished by two bidentate **L2** ligands, with a pyridine nitrogen atom (Cu1–N17, 2.030(3) Å), two indazole nitrogen atoms (Cu1–N9, 1.994(3) and Cu1–N24, 1.974(3) Å) and a nitrate oxygen atom (Cu1–O32, 2.029(3) Å) forming the basal plane and the remaining pyridine nitrogen atom situated at the apex (Cu1–N2, 2.216(3) Å). There is a slightly larger twist between the pyridine and indazole rings in **L2** compared to those found for **L1** in **1**, with interplanar angles of 12.8 and 11.7°, Fig. 4.

As was the case in **1**, π–π interactions pervade the extended structure of **2**. Two types of interactions are present: a chain that runs parallel to the crystallographic *b* axis formed by the partial overlap of **L2** ligands on adjacent molecules (interplanar distance 3.63 Å), and; the linking of these chains parallel to the crystallographic *a* axis by the face-to-face interaction between two equivalent **L2** units (interplanar distance 3.54 Å). No significant interactions are observed running parallel to the *c* axis.

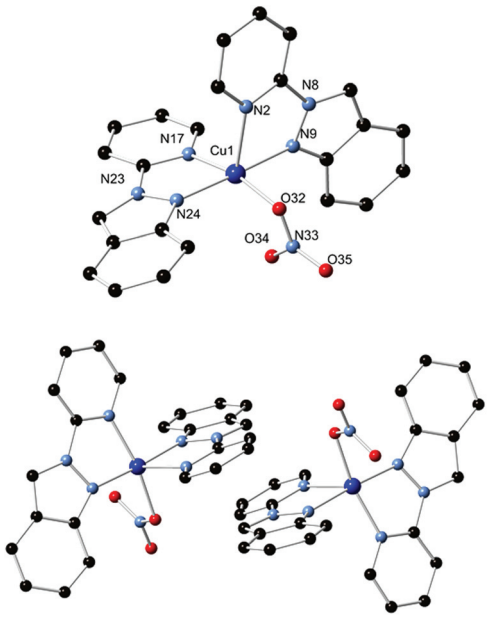

Fig. 4 Structure of **2** with heteroatom labelling scheme (top). Example of π–π interactions in the structure of **2** (bottom). Hydrogen atoms and non-coordinating nitrate anions omitted for clarity.

The observed differences in bond lengths in the free ligands are reduced on coordination to the copper ions in **1** and **2**, as evidenced by the statistically equivalent lengths of the ring junction bonds in **1** and **2**, each falling in the range 1.409(5)–1.425(4) Å. However, the C–C bond from the indazole 3-position to the adjacent ring junction carbon atom is marginally longer within **L1** in **1** (average 1.432(6) Å) compared with those in **L2** in **2** (average 1.393(5) Å). While the metal–ligand bond lengths cannot be directly compared between **1** and **2** due to their different coordination geometries, the similarity in their MLCT bands in the solution UV/Visible spectra suggest comparable metal-chromophores. While the two ligands still show differences in their electronic structures when coordinated, these differences likely play a smaller role in determining their metallo-supramolecular chemistry than does their significantly different steric profiles (**L1** angular, **L2** linear). These pronounced steric differences most likely dictate the coordination geometry and crystal packing of complexes **1** and **2**, especially where the barrier to conversion between square pyramidal and trigonal bipyramidal is sufficiently small to be influenced by crystal packing effects.

Synthesis and characterisation of Cu(II) complexes of H_2L3 and H_2L4: $[Cu_3(HL3)_4(NO_3)_2(EtOH)_2]\cdot 3C_6H_6\cdot 2H_2O$, 3, and $[Cu(HL4)_2]\cdot H_2O\cdot MeOH$, 4

Blue/green crystals of **3** deposited within one month after an ethanolic solution containing $\mathbf{H_2L3}$ and $Cu(NO_3)_2\cdot 3H_2O$ was subjected to the slow diffusion of benzene vapour. An immediate loss of single crystallinity was observed when these crystals were removed from their mother liquor, presumably due to the loss of included solvent molecules. Thermal analysis showed

the immediate onset of mass loss with three sequential mass losses totalling *ca.* 30% before 250 °C, consistent with the loss of included solvent molecules. These transitions led directly to decomposition and micro-analytical data for an air-dried sample were consistent with the rapid loss of benzene molecules on standing and suggest the following formulation: $[Cu_3(\mathbf{HL3})_4(NO_3)_2(EtOH)_2]\cdot 3(H_2O)$. Likewise, purple rod crystals of **4** deposit after several days when a methanolic solution of $\mathbf{H_2L4}$ and $Cu(NO_3)_2\cdot 3H_2O$ was allowed to stand. Air stable crystals of **4** were isolated by filtration and micro-analytical data were consistent with the following formulation: $[Cu(\mathbf{HL4})_2]\cdot H_2O\cdot MeOH$. The crystals of **3** and **4** were of sufficient quality to enable their structures to be determined by single crystal X-ray diffraction.

X-ray crystal structure of 3

The crystal data for **3** were solved and the structure model refined in the triclinic space group $P\bar{1}$ and crystallographic data are detailed in Table 1. The asymmetric unit contains two non-equivalent Cu(II) centres, both located on crystallographic special positions, Fig. 5. Cu1 is coordinated by four unique carboxylate oxygen atoms from two non-equivalent units of **HL3**, and one ethanol molecule in a square pyramidal arrangement, with the ethanol molecule occupying the axial position (Cu–O27 2.161(3) Å). Application of the crystallographic inversion reveals the archetypal $[Cu_2(OAc)_4]$ paddlewheel motif and results in the formation of a square planar-type node geometry for the coordinating **HL3** ligands. Cu2 is six coordinate with a distorted octahedral arrangement which is comprised from four monodentate indazole nitrogen atoms from two crystallographically unique **HL3** units occupying the equatorial plane, and disordered nitrate anions coordinating in the elongated axial positions with Cu2–O30 distance 2.373(3) Å. Also present within the crystal lattice are two water molecules (per three Cu(II) ions) that hydrogen bond to half of the protonated indazole nitrogen atoms, while the remaining protonated indazole nitrogen atoms donate hydrogen bonds to one of the disordered nitrate anions, along with one benzene molecule per Cu(II) ion. With ligand **HL3** acting as a 2-connected linear bridge, and considering the entire paddlewheel cluster as a node, the network of **3** can be described as a (4,4) 2-dimensional sheet, Fig. 6.

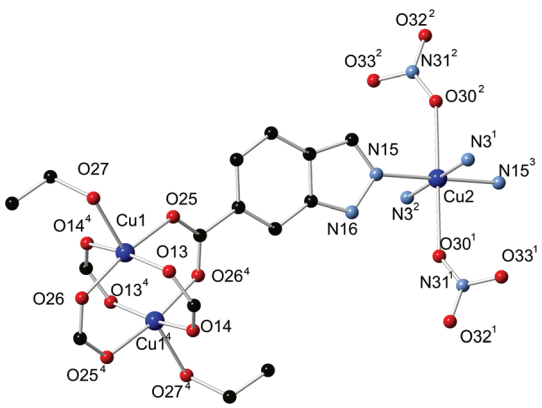

Fig. 5 Copper coordination environments of one **HL3** ligand in **3** with heteroatom labelling scheme. Hydrogen atoms, nitrate anion disorder and lattice solvent molecules omitted for clarity. Symmetry codes used to generate equivalent atoms: (1) 1 + *X*, 1 + *Y*, +*Z*; (2) 2 – *X*, 2 – *Y*, –*Z*; (3) 3 – *X*, 3 – *Y*, –*Z*; (4) 3 – *X*, 2 – *Y*, 1 – *Z*.

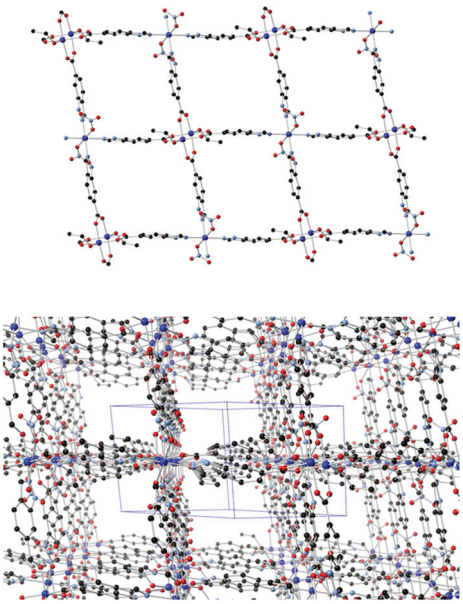

Fig. 6 Structure of a single (4,4) sheet in **3** (top). Packing diagram showing solvent channel in **3**, with unit cell overlay (bottom). Hydrogen atoms, lattice solvent molecules and anion disorder omitted for clarity.

Adjacent sheets are stacked in such a way as to form square-walled one-dimensional channels, with interatomic dimensions approximately 9 × 11 Å. These channels pass through the framework windows parallel to the [0,1,1] vector, and the benzene and non-coordinating water molecules within this channel occupy approximately 37% of the unit cell volume. The aromatic rings of **HL3** are oriented orthogonal to the mean plane of the sheet, while the bulk of hydrogen bonding is observed within the sheets, limiting any interaction between the sheets to weak hydrogen bonding between the coordinating ethanol molecule and one orientation of the disordered nitrate molecule of the adjacent sheet.

X-ray crystal structure of 4

The crystal data for **4** were solved and the structure model refined in the triclinic space group *C*2/*c* and crystallographic data are detailed in Table 1. Analysis revealed one Cu(II) ion, coordinating to two equivalent chelating molecules of **HL4** in a *trans*-square planar arrangement, where the ligand mean planes are parallel. While **HL4** formally adopts the 2*H*-tautomeric configuration in the structure of **4**, no significant deviations to the ring junction or adjacent carbon–carbon bond lengths were observed when compared to those seen in the free ligand, especially when consideration is given to the struc-

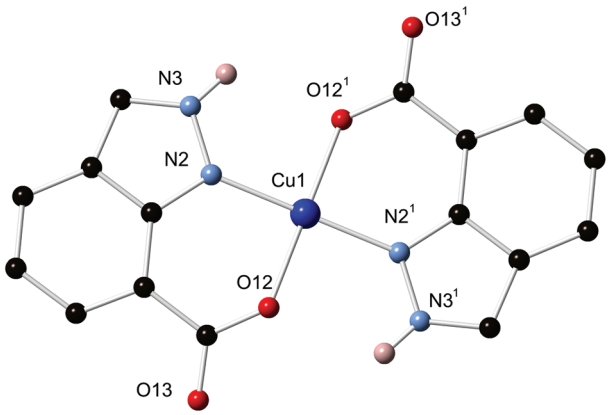

Fig. 7 Structure of **4** with heteroatom labelling scheme. Selected hydrogen atoms and lattice solvent molecules omitted for clarity. Symmetry codes used to generate equivalent atoms: (1) 1 − *X*, −*Y*, 1 − *Z*.

tural changes brought about by deprotonation and chelation. Also located within the unit cell was one molecule of water per Cu(II) ion, and one methanol molecule, disordered over two equivalent orientations, Fig. 7.

The intermolecular interactions in **4** are dominated by hydrogen bonding, where indazole nitrogen atom N3 donates a hydrogen bond to the lattice water molecule, which itself donates a hydrogen bond to carboxylate oxygen atom O13. These two interactions are replicated by crystallographic symmetry, with the result that the lattice water molecule acts as a hydrogen-bonded bridge between [Cu(**HL4**)] moieties, and participates in four hydrogen bond interactions: two as a donor and two as an acceptor. Interestingly, this mode of hydrogen bonding is similar to that seen in the structure of the free ligand hydrate, where *in lieu* of the reciprocating N–H···O hydrogen bonds holding two units of the free ligand together, the square planar Cu(II) ion achieves the same result, with N2–O12 distance of 2.687(3) Å only slightly shorter than the equivalent distances in the free ligand structure of 2.816(2) and 2.825(2) Å. As was the case in the free ligand, these interactions propagate a 1D chain that runs parallel to the crystallographic *a* unit cell axis, Fig. 8. Adjacent chains align by way of parallel π–π stacking interactions on each face of the complex, at mean interplanar separation of 3.32 Å. Similar to the case in the free ligand structure, the aromatic ring planes are directly above the metal ions of adjacent chains, providing little overlap with the aromatic systems of the ligands. The disordered methanol molecules also donate hydrogen bonds to carboxylate oxygen atom O13, but do not contribute to the topological description of the complex.

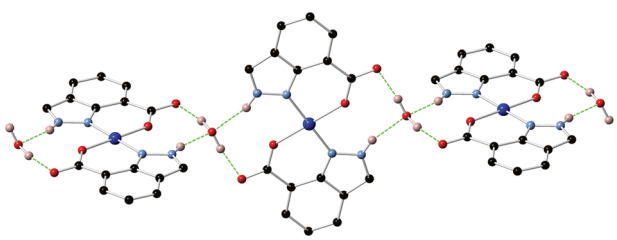

Fig. 8 Structure of the hydrogen-bonded chain present in **4**. Selected hydrogen atoms and lattice solvent molecules omitted for clarity.

Conclusions

The foregoing results demonstrate the versatility of the heterocyclic indazole ring system to further functionalization to give ligands capable of forming interesting metallo-supramolecular assemblies. Substitution of a 2-pyridyl group at the 1- or 2-positions of the indazole backbone gave the two tautomerically related *N*,*N*-bidentate chelating ligands **L1** and **L2**, respectively. The coordination of two of these ligands about Cu(II) in **1** and **2** led to the formation of five-coordinate complexes whereby a nitrate ion completed the coordination sphere. While **1** and **2** have identical N_4O-coordination spheres their geometries differ from distorted trigonal bipyramidal to square pyramidal. The different geometric outcomes can be traced to the differences in the conformational shapes of the coordinating ligands, with **L1** and **L2** presenting 'angular' and 'linear' profiles, respectively. These ligand profiles influence the way in which **1** and **2** interact throughout the crystal lattice *via* π–π stacking interactions. Enhancing these interactions probably has greater bearing on the coordination geometries than does any subtle electronic change brought about by the different substitution patterns in **L1** and **L2**.

Substitution of carboxylic acid groups to the 6- or 7-positions of the indazole ring skeleton gave ligands $\mathbf{H_2L3}$ and $\mathbf{H_2L4}$ capable of divergent and chelating coordination geometries, respectively. In both cases the substantial impact of hydrogen bonding was obvious, bought about by the hydrogen bond donor sites directly adjacent to the coordinating sites at tautomerically related positions in Cu(II) complexes **3** and **4**. These structural features reiterate the beneficial properties to ligand design of both the 1,2-diazole skeleton and the fused bicyclic feature of the indazole framework, allowing access to unusual coordination geometries as well as favourable sites for strong hydrogen bond interactions.

The preceding results also show a clear indication of dimensionality control by substitution pattern. Substitution of coordination functionality at the 1- and 2-positions of the indazole ring leads to convergent chelating ligands, obviously resulting in the formation of discrete assemblies. Substitution of carboxylate functionality at the 7-position leads to a chelating, convergent arrangement which is augmented by hydrogen bonding functionality, combining a chelating coordination geometry with a divergent supramolecular synthon. Substitution at the 6-position, as expected, leads exclusively to higher dimensionality assemblies by virtue of the divergent orientation of coordinating groups. Work in our laboratory studying the coordination chemistry of these and related ligand systems is ongoing as well investigating the effects of introducing further substitution onto heterocyclic ligands, and will be reported in due course.

Acknowledgements

The authors gratefully acknowledge the University of Canterbury (College of Science scholarship to CSH) and the Royal Society of New Zealand Marsden Fund for financial support. The authors thank Dr Anthea Lees for helpful discussions.

Notes and references

1 J. W. Steed and J. L. Atwood, *Supramolecular Chemistry*, Wiley-VCH, Weinheim, 2nd edn, 2009; *Metal-Organic Frameworks: Design and Application*, ed. L. R. MacGillivray, Wiley-VCH, Weinheim, 2010; J. F. Ayme, J. E. Beves, D. A. Leigh, R. T. McBurney, K. Rissanen and D. Schultz, *Nat. Chem.*, 2012, **4**, 15–20; Y. Inokuma, S. Yoshioka, J. Ariyoshi, T. Arai, Y. Hitora, K. Takada, S. Matsunaga, K. Rissanen and M. Fujita, *Nature*, 2013, **495**, 461–466; H. C. Zhou, J. R. Long and O. M. Yaghi, *Chem. Rev.*, 2012, **112**, 673–674.

2 V. Guillerm, L. J. Weseliński, Y. Belmabkhout, A. J. Cairns, V. D'Elia, L. Wojtas, K. Adil and M. Eddaoudi, *Nat. Chem.*, 2014, **6**, 673–680; K. Sumida, D. L. Rogow, J. A. Mason, T. M. McDonald, E. D. Bloch, Z. R. Herm, T. H. Bae and J. R. Long, *Chem. Rev.*, 2012, **112**, 724–781; M. B. Duriska, S. M. Neville, B. Moubaraki, J. A. Cashion, G. J. Halder, K. W. Chapman, C. Balde, J. F. Letard, K. S. Murray, C. J. Kepert and S. R. Batten, *Angew. Chem., Int. Ed.*, 2009, **48**, 2549–2552; A. Ferguson, M. A. Squire, D. Siretanu, D. Mitcov, C. Mathoniere, R. Clerac and P. E. Kruger, *Chem. Commun.*, 2013, **49**, 1597–1599; R. A. Smaldone, R. S. Forgan, H. Furukawa, J. J. Gassensmith, A. M. Z. Slawin, O. M. Yaghi and J. F. Stoddart, *Angew. Chem., Int. Ed.*, 2010, **49**, 8630–8634.

3 S.-Q. Bai, D. J. Young and T. S. A. Hor, *Chem. – Asian. J.*, 2011, **6**, 292–304; M. Du, C.-P. Li, C.-S. Liu and S.-M. Fang, *Coord. Chem. Rev.*, 2013, **257**, 1282–1305; P. J. Steel, *Acc. Chem. Res.*, 2005, **38**, 243–250.

4 P. Nugent, Y. Belmabkhout, S. D. Burd, A. J. Cairns, R. Luebke, K. Forrest, T. Pham, S. Ma, B. Space, L. Wojtas, M. Eddaoudi and M. J. Zaworotko, *Nature*, 2013, **495**, 80–84; S. Noro, S. Kitagawa, M. Kondo and K. Seki, *Angew. Chem., Int. Ed.*, 2000, **39**, 2082–2084; N. R. Kelly, S. Goetz, S. R. Batten and P. E. Kruger, *CrystEngComm*, 2008, **10**, 1018–1026.

5 K. E. Knope, H. Kimura, Y. Yasaka, M. Nakahara, M. B. Andrews and C. L. Cahill, *Inorg. Chem.*, 2012, **51**, 3883–3890; P. King, R. Clerac, C. E. Anson and A. K. Powell, *Dalton Trans.*, 2004, 852–861; K. V. Domasevitch, I. Boldog, E. B. Rusanov, J. Hunger, S. Blaurock, M. Schroeder and J. Sieler, *Z. Anorg. Allg. Chem.*, 2005, **631**, 1095–1100; J.-P. Zhang, S. Horike and S. Kitagawa, *Angew. Chem., Int. Ed.*, 2007, **46**, 889–892; A. Goswami, S. Sengupta and R. Mondal, *CrystEngComm*, 2012, **14**, 561–572; C. S. Hawes and P. E. Kruger, *Aust. J. Chem.*, 2013, **66**, 401–408.

6 M. Zhang, M. Bosch, T. Gentle III and H.-C. Zhou, *CrystEngComm*, 2014, **16**, 4069–4083.

7 V. Colombo, S. Galli, H. J. Choi, G. D. Han, A. Maspero, G. Palmisano, N. Masciocchi and J. R. Long, *Chem. Sci.*, 2011, **2**, 1311–1319.

8 T. Eicher, S. Hauptmann and A. Speicher, *The Chemistry of Heterocycles: Structure, Reactions, Syntheses, and Applications*, Wiley-VCH, Weinheim, 2003; A. Schmidt, A. Beutler and B. Snovydovych, *Eur. J. Org. Chem.*, 2008, 4073–4095.

9 C. Pettinari, F. Marchetti, S. Orbisaglia, R. Pettinari, J. Ngoune, M. Gomez, C. Santos and E. Alvarez, *CrystEngComm*, 2013, **15**, 3892–3907; A. J. Canty, A. Dedieu, H. Jin, A. Milet, B. W. Skelton, S. Trofimenko and A. H. White, *Inorg. Chim. Acta*, 1999, **287**, 27–36; R. Pettinari, C. Pettinari, F. Marchetti, R. Gobetto, C. Nervi, M. R. Chierotti, E. J. Chan, B. W. Skelton and A. H. White, *Inorg. Chem.*, 2010, **49**, 11205–11215; C. Janiak, S. Temizdemir, S. Dechert, W. Deck, F. Girgsdies, J. Heinze, M. J. Kolm, T. G. Scharmann and O. M. Zipffel, *Eur. J. Inorg. Chem.*, 2000, 1229–1241; J. C. Cuevas, J. Demendoza, P. Prados, F. Hernandezcano and C. Focesfoces, *J. Chem. Soc., Chem. Commun.*, 1986, 1641–1642; I. N. Stepanenko, A. A. Krokhin, R. O. John, A. Roller, V. B. Arion, M. A. Jakupec and B. K. Keppler, *Inorg. Chem.*, 2008, **47**, 7338–7347.

10 R. Pritchard, C. A. Kilner and M. A. Halcrow, *Tetrahedron Lett.*, 2009, **50**, 2484–2486.

11 C. S. Hawes, R. Babarao, M. R. Hill, K. F. White, B. F. Abrahams and P. E. Kruger, *Chem. Commun.*, 2012, **48**, 11558–11560.

12 C. S. Hawes and P. E. Kruger, *RSC Adv.*, 2014, **4**, 15770–15775.

13 G. M. Sheldrick, *Acta Crystallogr., Sect. A: Fundam. Crystallogr.*, 2008, **64**, 112–122.

14 G. M. Sheldrick, *SHELXL-97, Programs for X-ray Crystal Structure Refinement*, University of Gottingen, 1997.

15 O. V. Dolomanov, L. J. Bourhis, R. J. Gildrea, J. A. K. Howard and H. Puschmann, *J. Appl. Crystallogr.*, 2009, **42**, 339–341.

16 S. A. A. Zaidi, S. S. Siddiqui and K. S. Siddiqui, *Transition Met. Chem.*, 1993, **18**, 51–54.

17 C. M. Fitchett, C. Richardson and P. J. Steel, *Org. Biomol. Chem.*, 2005, **3**, 498–502.

18 J. Catalan, J. C. Delvalle, R. M. Claramunt, G. Boyer, J. Laynez, J. Gomez, P. Jimenez, F. Tomas and J. Elguero, *J. Phys. Chem.*, 1994, **98**, 10606–10612.

19 L. Golic, I. Leban, B. Stanovnik, M. Tisler and A. Tomazic, *Croat. Chem. Acta*, 1980, **53**, 435–440; F. Shibahara, A. Kitagawa, E. Yamaguchi and T. Murai, *Org. Lett.*, 2006, **8**, 5621–5624.

20 B. J. Hathaway, *Coord. Chem. Rev.*, 1970, **5**, 143–207.

21 F. Jacobson and L. Huber, *Chem. Ber.*, 1908, **41**, 660–671.

22 A. W. Addison, T. N. Rao, J. Reedijk, J. van Rijn and G. C. Verschoor, *J. Chem. Soc., Dalton Trans.*, 1984, 1349–1356.

